ELSEVIER

Journal of Molecular Catalysis A: Chemical 182–183 (2002) 185–193

JOURNAL OF MOLECULAR CATALYSIS A: CHEMICAL

www.elsevier.com/locate/molcata

Bulk redox properties of heteropolyacids determined from surface properties of nanostructured heteropolyacid monolayers

In K. Song[1], Mark A. Barteau*

Department of Chemical Engineering, Center for Catalytic Science and Technology, University of Delaware, Newark, DE 19716, USA

Received 12 July 2001; accepted 23 October 2001

Abstract

Bulk redox properties of Keggin-type heteropolyacids (HPAs) were determined from surface properties of nanostructured HPA monolayers using scanning tunneling microscopy (STM) and tunneling spectroscopy (TS). Cation-exchanged $R_nPMo_{12}O_{40}$ ($R = H^+, Cs^+, Ba^{2+}, Zn^{2+}, Co^{2+}, Cu^{2+}, Bi^{3+}$), polyatom-substituted $H_nPW_{11}MO_{40}$ ($M = W^{6+}, Mo^{6+}, V^{5+}$) and heteroatom-substituted $H_nXW_{12}O_{40}$ ($X = P^{5+}, Si^{4+}, B^{3+}, Co^{2+}$) HPAs were examined to elucidate the effect of different substitutions. All HPA samples formed two-dimensional well-ordered monolayer arrays and exhibited negative difference resistance (NDR) behavior in their tunneling spectra. In all cases NDR peaks appeared at less negative potentials for higher reduction potentials of the HPAs. These changes could also be correlated with the electronegativity of the substituted atoms. Substitution of more electronegative atoms for counter-cations or central heteroatoms shifted the NDR peaks to less negative voltages, corresponding to increased reduction potentials of the HPAs. However, substitution of more electronegative metals into the Keggin framework shifted the NDR peaks to more negative voltages, corresponding to decreased reduction potentials.

Keywords: Heteropolyacid; Scanning tunneling microscopy; Negative differential resistance; Reduction potential; Electronegativity

1. Introduction

Scanning tunneling microscopy (STM) has shown tremendous potential for observing ordered molecular structures [1–5], and has provided direct insights to chemical reactions on single crystal metal surfaces [6–8]. Direct imaging of adsorbed molecules on catalyst surfaces is of importance in understanding chemical reaction pathways and reaction sites on surfaces. Examples of adsorbates imaged on metal surfaces include carbon monoxide on Rh(1 1 1) [9] and Ag(1 1 0) [10], oxygen on Pd(1 1 1) [11] and Pt(1 1 1) [12,13], benzoic acid on Cu(1 1 0) [14] and methoxy and formate species on Cu(1 1 0) [15]. The STM image is a convolution of both the geometric and electronic structures of surfaces and adsorbates. However, tunneling spectroscopy (TS) probes only electronic states of surface species and has been utilized as a technique to distinguish between different molecules with very similar geometric structures and molecular sizes [15–17]. For example, individual molecules of soccer ball-like $H_3PW_{12}O_{40}$ and $H_3PMo_{12}O_{40}$ (whose molecular structures and dimensions are nearly identical) in mixed arrays could be

* Corresponding author. Tel.: +1-302-831-8905; fax: +1-302-831-8201.
E-mail address: barteau@che.udel.edu (M.A. Barteau).
[1] Present address: Department of Industrial Chemistry, Kangnung National University, Kangnung 210-702, Korea.

1381-1169/02/$ – see front matter © 2002 Elsevier Science B.V. All rights reserved.
PII: S1381-1169(01)00466-6

successfully distinguished by their TS responses [18]. Moreover, TS measured for a single organic molecule on a metal surface, e.g. C_2H_2 on Cu(1 0 0), has proven to be a valuable spectroscopic technique (referred to as single-molecule vibrational spectroscopy and microscopy) to fingerprint the identity of the organic molecule [19].

Heteropolyacids (HPAs), also known as polyoxometalates (POMs), are early transition metal oxygen anion clusters that exhibit a wide range of molecular sizes, compositions and architectures [20,21]. Among various HPA structural classes, the Keggin-type [22] HPAs have been widely employed as catalysts in homogeneous and heterogeneous systems for acid–base and oxidation reactions [23–26]. Some of these reactions include hydration of propene [27], *n*-butene [28], and isobutene [29], polymerization of tetrahydrofuran [30], oxidation of methacrolein [31] and Wacker and related olefin oxidations [32]. One of the great advantages of HPA catalysts is that their catalytic properties can be tuned by changing the identity of charge-compensating counter-cations, heteroatoms and framework metal atoms (polyatoms) [33].

Recently, members of four HPA structural classes, Keggin- [22], Wells–Dawson- [34], Finke–Droege- [35], and Pope–Jeannin–Preyssler-type [36] HPAs, have been successfully imaged in air using STM by depositing these molecules on graphite surfaces [37]. Previous STM studies of HPAs showed that two-dimensional ordered arrays of these molecules on a graphite surface exhibited a distinctive current–voltage (*I–V*) behavior referred to as negative differential resistance (NDR) in their tunneling spectra [37–46]. Simple one-dimensional theory predicts that the transmission probability between two electronically equivalent electrodes should increase monotonically with increasing applied potential [47]. NDR behavior is manifested as local maxima and minima in an *I–V* spectrum. Such peaks in the *I–V* spectrum result in negative values of d*I*/d*V*, and thus the phenomenon is referred to as NDR. NDR behavior has been explained in terms of resonant tunneling through a double barrier quantum well [48,49], and has been observed consistently for the arrays of pure HPAs [37–46]. We have shown that NDR peak voltages of HPAs are closely related to the electronic properties of HPAs and in turn to the redox potentials of HPAs [40–44]. NDR peak voltages can be influenced by the identity of the counter-cations [40–42], framework transition metal atoms [41–43], heteroatoms [44] and adsorbed organic molecules [45,46]. Although at present the correlations between NDR peak voltages and redox properties of HPAs are largely qualitative, it may be possible in the future to construct quantitative relationships. The development of such relationships will require better theoretical understanding of the origin of the NDR phenomenon in these molecules, as well as experimental results testing a wide range of HPA compositions and structures.

Reported in this work is a comprehensive investigation of bulk redox properties of HPAs determined from surface properties of nanostructured HPA monolayers using STM. Keggin-type [22] HPAs with different counter-cation, polyatom and heteroatom substitutions were examined. HPA samples were deposited on a highly oriented pyrolytic graphite (HOPG) surface in order to obtain images and tunneling spectra. The observed NDR peak voltages of HPA monolayers were correlated with the redox properties of the HPAs as well as with the electronegativities of the substituted atoms.

2. Experimental

2.1. Sample preparation and deposition

Cation-exchanged $R_nPMo_{12}O_{40}$ ($R = H^+$, Cs^+, Ba^{2+}, Zn^{2+}, Co^{2+}, Cu^{2+}, Bi^{3+}), polyatom-substituted $H_nPW_{11}MO_{40}$ ($M = W^{6+}$, Mo^{6+}, V^{5+}) and heteroatom-substituted $H_nXW_{12}O_{40}$ ($X = P^{5+}$, Si^{4+}, B^{3+}, Co^{2+}) HPAs were investigated. Commercially available $H_3PMo_{12}O_{40}$, $H_3PW_{12}O_{40}$ and $H_4SiW_{12}O_{40}$ samples were obtained from Aldrich Chemical. $H_3PW_{11}Mo_1O_{40}$ and $H_4PW_{11}V_1O_{40}$ were purchased from Nippon Inorganic Color and Chemicals. $H_5BW_{12}O_{40}$ and $H_6CoW_{12}O_{40}$ were provided by Prof. Craig L. Hill at Emory University. Cation-exchanged HPAs were prepared by replacing all protons of $H_3PMo_{12}O_{40}$ with metal atoms according to published methods [50,51]. Approximately 0.01 M aqueous solutions of each HPA sample were prepared. A drop of solution was deposited on a freshly cleaved HOPG surface and allowed to dry in air for ca. 1 h at room temperature for STM imaging and TS measurements.

2.2. STM and TS

STM images were obtained in air using a Topometrix TMX 2010 instrument. Mechanically formed Pt/Ir (90/10) tips were used as probes. Scanning was done in the constant current mode at a positive sample bias of 100 mV and tunneling current of 1–2 nA. Tunneling spectra were measured in air. Both Topometrix TMX 2010 and LK Technologies LK-1000 STM instruments were used to confirm consistency and reproducibility of tunneling spectra. STM tips were first calibrated by imaging bare HOPG to confirm its standard periodicity (2.46 Å). Several tunneling spectra were then taken on the bare graphite section of the surface to ensure the stability of the tip and the reproducibility of the tunneling spectrum of HOPG. Once these had been established, the tip would be moved to the HPA-covered section to image and obtain tunneling spectra of the HPA sample. To measure a tunneling spectrum, the sample bias was ramped from -2 to $+2$ V with respect to the tip and the tunneling current was monitored. The voltage axis in the tunneling spectrum represents the potential applied to the sample relative to that of the tip. TS measurements were performed at least 10 times each using at least three different tips for each sample to obtain more accurate and reproducible results and provide a basis for statistical analyses.

3. Results and discussion

3.1. Two-dimensional well-ordered monolayer arrays

Fig. 1(a) shows the molecular structure of the pseudo-spherical (T_d symmetry) Keggin-type $[PMo_{12}O_{40}]^{3-}$ heteropolyanion [52]. The structure of $[PMo_{12}O_{40}]^{3-}$ consists of a heteroatom, P, at the center of the anion cluster, tetrahedrally coordinated to four oxygen atoms. This tetrahedron is surrounded by 12 MoO_6 octahedra. The van der Waals diameter along the 3-fold axis of symmetry (i.e. the vertical dimension of the structure in Fig. 1(a)) is 11.97 Å [52–54]. Fig. 1(b) shows the three-dimensional array of HPAs comprising heteropolyanions, protons, cations, water and/or organic molecules called the secondary structure [24]. The counter-cations are located in the interstitial spaces between heteropolyanions. The primary structure, the Keggin structure [22], of the heteropolyanion is relatively stable and insensitive to its surroundings. However, the secondary structure is very labile and may change in different environments by either increasing or decreasing the interstitial space between heteropolyanions.

Fig. 2 shows the STM image and unit cell of a $H_3PMo_{12}O_{40}$ array on graphite. The STM image clearly shows the formation of a self-assembled

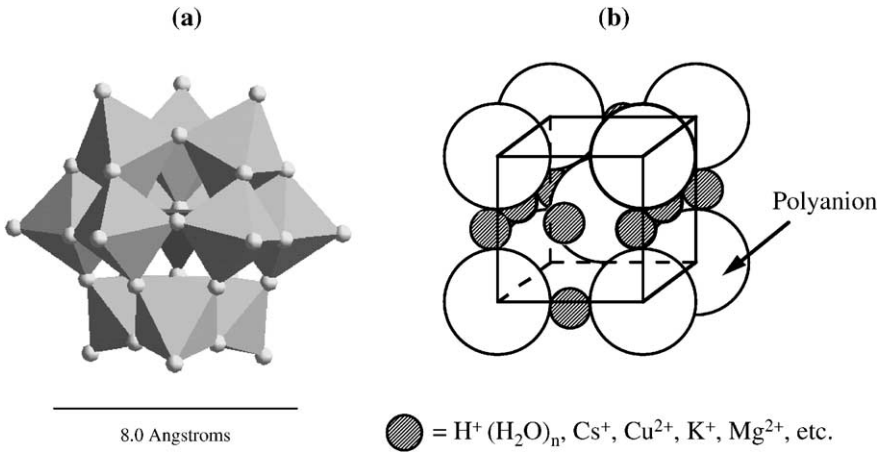

Fig. 1. (a) Polyhedral representation of the molecular structure of $[PMo_{12}O_{40}]^{3-}$ heteropolyanion [52] and (b) schematic diagram of the secondary structure of HPAs [24].

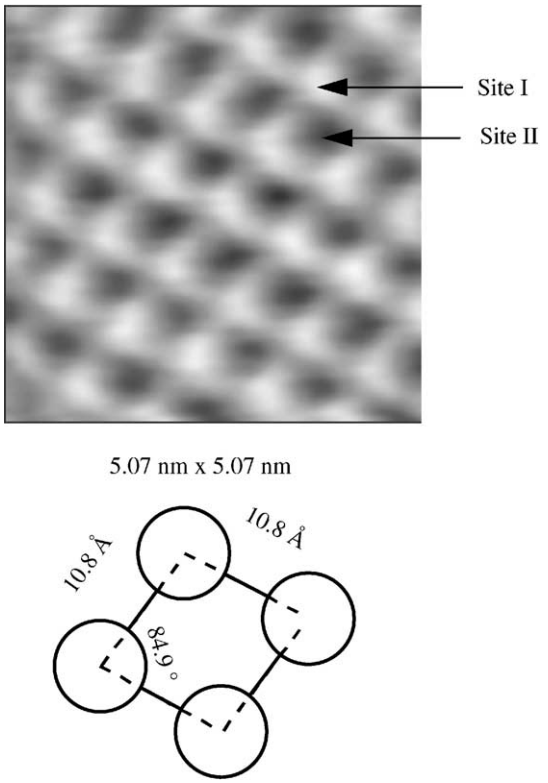

Fig. 2. STM image and unit cell of $H_3PMo_{12}O_{40}$ array on graphite.

and well-ordered array on the graphite surface. The periodicity and included angle of the unit cell constructed on the basis of lattice constants determined from two-dimensional fast Fourier transform (2-D FFT) are 10.8 Å and 84.9°, respectively. The measured periodicity is in good agreement with lattice constants of the Keggin-type HPAs obtained by STM [37–46] and X-ray crystallography [52–54]. All HPA samples examined in this work formed well-ordered arrays on graphite surfaces over scan areas of at least 200 Å × 200 Å.

Fig. 3 shows the typical tunneling spectra taken at two different sites, denoted as Site I and Site II in the image of the $H_3PMo_{12}O_{40}$ array in Fig. 2. The spectrum taken at a position corresponding to the bright corrugation (Site I) exhibits a distinctive *I–V* behavior, referred to as NDR, showing an NDR peak at −0.95 V. The NDR peak voltage was defined as the voltage at which the maximum current was observed in this region. A tunneling spectrum taken at the

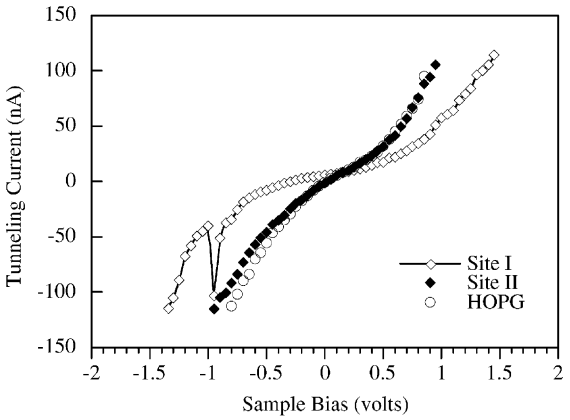

Fig. 3. *I–V* spectra taken at two different sites (Site I and Site II) in the STM image of $H_3PMo_{12}O_{40}$ in Fig. 2.

interstitial space (Site II) between bright corrugations showed the same *I–V* response as bare graphite indicating that the two-dimensional array of $H_3PMo_{12}O_{40}$ on graphite is a monolayer, as previously demonstrated [37–46]. The NDR measurements atop the bright corrugations (Site I) were carried out several times with at least three different tips to obtain more accurate and reproducible results and provide a basis for statistical analyses. Fig. 4 shows the frequency and monomodal distribution of NDR peak voltages of the $H_3PMo_{12}O_{40}$ sample. The statistical average of NDR peak voltage of the $H_3PMo_{12}O_{40}$ array was found to

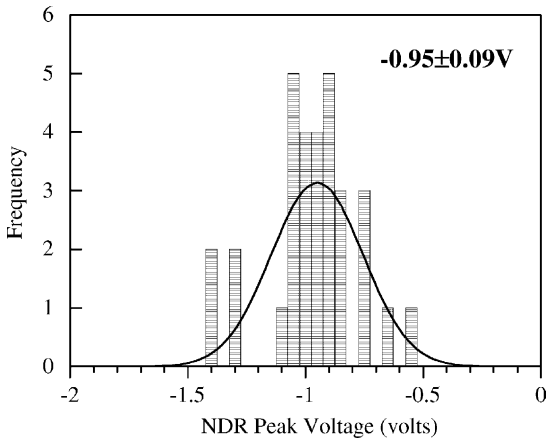

Fig. 4. Frequency and monomodal distribution of NDR peak voltages of $H_3PMo_{12}O_{40}$ monolayer showing a statistical mean of -0.95 ± 0.09 V.

be -0.95 ± 0.09 V. The most reproducible and representative NDR peak voltage of each HPA sample examined in this work was determined in this way.

3.2. Effect of counter-cation substitution

The STM measurements in this work were done at positive sample biases with respect to the tip. This means that electrons flow from tip to sample in the normal mode of operation. NDR behavior in the tunneling spectra of HPAs is observed at negative sample biases, i.e. when electrons tunnel from sample to tip. We have demonstrated that the striking NDR behavior of nanostructured HPA arrays measured by STM may be closely related to the electronic properties of these materials, and may serve as a fingerprint of their redox properties [40–44]. Previous results [40–42] have shown that the NDR peaks appeared at less negative applied voltages when the protons of the $H_3PMo_{12}O_{40}$ were replaced by more electronegative cations such as Cu^{2+}; the NDR peaks shifted to higher negative voltages when the protons were replaced by less electronegative cations such as Cs^+ [40]. When the reduction potentials of cation-exchanged HPAs were plotted against the electronegativities of the counter-cations defined by Tanaka and Ozami [55], it became apparent that as more electronegative cations were substituted for less electronegative ones, the reduction potential increased and vice versa [50].

Comprehensive trends of reduction potential of cation-exchanged HPAs and electronegativity of counter-cations with respect to NDR peak voltages of the HPAs were well established by investigating a set of cation-exchanged $R_nPMo_{12}O_{40}$ ($R = H^+$, Cs^+, Ba^{2+}, Zn^{2+}, Co^{2+}, Cu^{2+}, Bi^{3+}) HPAs, which cover a wide range of Tanaka electronegativities [55] of counter-cations. Fig. 5 shows the reciprocal reduction temperature of cation-exchanged HPAs taken from the literature [50] and the Tanaka electronegativity [55] of the counter-cations, both plotted with respect to the NDR peak voltages of cation-exchanged HPAs. The NDR peak voltages observed for cation-exchanged HPAs appeared at less negative values with decreasing reduction temperature of HPAs and increasing electronegativity of the counter-cation. In other words, the HPA salts with more electronegative counter-cations had higher reduction potentials and showed NDR behavior at less negative applied voltages. The Tanaka

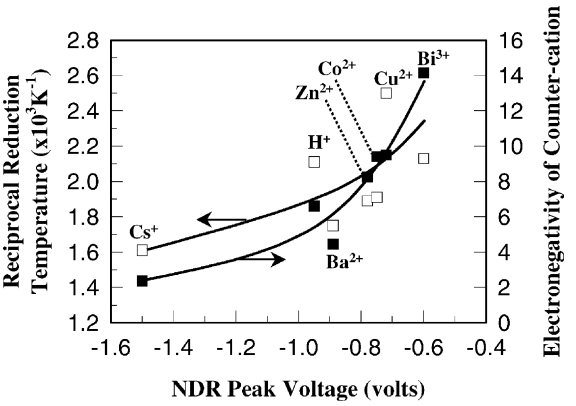

Fig. 5. Correlation between NDR peak voltage of cation-exchanged $R_nPMo_{12}O_{40}$ ($R = H^+$, Cs^+, Ba^{2+}, Zn^{2+}, Co^{2+}, Cu^{2+}, Bi^{3+}) HPAs and Tanaka electronegativity [55] of the counter-cation (filled squares), and between NDR voltage and reciprocal reduction temperature [50] of $R_nPMo_{12}O_{40}$ ($R = H^+$, Cs^+, Ba^{2+}, Zn^{2+}, Co^{2+}, Cu^{2+}, Bi^{3+}) samples (open squares).

electronegativity [55] takes into account the electron donating and accepting ability of the atom. One explanation for these results is that a more electronegative cation acts as a large electron reservoir to facilitate electron transfer to the heteropolyanion in reducing environments, by providing a route for electron delocalization [56].

3.3. Effect of heteroatom substitution

Fig. 6 shows the correlation between NDR peak voltage of heteroatom-substituted $H_nXW_{12}O_{40}$ ($X = P^{5+}$, Si^{4+}, B^{3+}, Co^{2+}) HPAs and Tanaka electronegativity of the heteroatom, and between NDR voltage and reduction potential of $H_nXW_{12}O_{40}$ ($X = P^{5+}$, Si^{4+}, B^{3+}, Co^{2+}) samples. Reduction potentials of $H_nXW_{12}O_{40}$ ($X = P^{5+}$, Si^{4+}, B^{3+}, Co^{2+}) HPAs were taken from the literature [33,57,58]. The NDR peak voltages of $H_nXW_{12}O_{40}$ ($X = P^{5+}$, Si^{4+}, B^{3+}, Co^{2+}) arrays appeared at less negative values with increasing reduction potential of the HPAs and increase in the electronegativity of the heteroatom. This result supports our general conclusion that more reducible HPAs show NDR behavior at less negative applied voltages in their tunneling spectra. Interestingly, the NDR peak voltage appears at a less negative value, and reduction potential increases with the increase in the

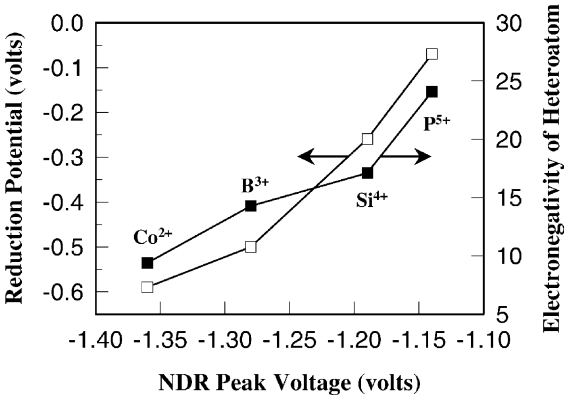

Fig. 6. Correlation between NDR peak voltage of heteroatom-substituted $H_nXW_{12}O_{40}$ ($X = P^{5+}$, Si^{4+}, B^{3+}, Co^{2+}) HPAs and Tanaka electronegativity [55] of the heteroatom (filled squares), and between NDR voltage and reduction potential [33,57,58] of $H_nXW_{12}O_{40}$ ($X = P^{5+}$, Si^{4+}, B^{3+}, Co^{2+}) samples (open squares).

electronegativity of the heteroatom in $H_nXW_{12}O_{40}$ ($X = P^{5+}$, Si^{4+}, B^{3+}, Co^{2+}). These NDR peak voltage and reduction potential dependencies on the electronegativity of heteroatoms exhibit exactly the same trends as those observed for cation-exchanged HPAs (Fig. 5). When taking into account different electron donating and accepting ability of the heteroatoms, however, the role and effect of heteroatom on the reduction potential of HPAs may be understood in a similar manner as suggested above for cation-exchanged HPAs.

In a previous study [59] investigating a set of heteroatom-substituted $H_nXMo_{12}O_{40}$ ($X = As^{5+}$, P^{5+}, Ge^{4+}, Si^{4+}) HPAs, it was demonstrated that reduction potentials of the HPAs (determined by polarographic methods) increased in the following order: Si^{4+} (0.475 V) < Ge^{4+} (0.492 V) < P^{5+} (0.518 V) < As^{5+} (0.526 V). According to a quantum-chemical calculation for $H_3PMo_{12}O_{40}$ by the Xα method, the LUMO (lowest unoccupied molecular orbital) is a mixture of 4d-orbitals of Mo (50%) and 2p-orbitals of the bridging oxygen atoms (50%), while the HOMO (highest occupied molecular orbital) is mostly composed of 2p-orbitals of bridging oxygen [60]. Theoretical calculations for $H_nXMo_{12}O_{40}$ ($X = As^{5+}$, P^{5+}, Ge^{4+}, Si^{4+}) HPAs revealed that the LUMO (antibonding with respect to Mo–O–Mo bonds) is responsible for reduction of HPAs and the reduction takes place at the bridging oxygens [59]. The calculated energy values of the LUMO for $H_nXMo_{12}O_{40}$ ($X = As^{5+}$, P^{5+}, Ge^{4+}, Si^{4+}) HPAs ranged between 18 and 20 eV below the vacuum level and followed the order $Si^{4+} > Ge^{4+} > P^{5+} > As^{5+}$, suggesting that $H_3AsMo_{12}O_{40}$ is the most reducible and $H_4SiMo_{12}O_{40}$ is the least reducible. Simple calculation of the Tanaka electronegativity of the heteroatom in these HPAs gives the sequence Si^{4+} (17.1) < Ge^{4+} (18.1) < As^{5+} (24.0) ≈ P^{5+} (24.1). Once again, reduction potential dependence of the $H_nXMo_{12}O_{40}$ ($X = As^{5+}$, P^{5+}, Ge^{4+}, Si^{4+}) HPAs on the electronegativity of the heteroatoms is roughly consistent with that observed for $H_nXW_{12}O_{40}$ ($X = P^{5+}$, Si^{4+}, B^{3+}, Co^{2+}) HPAs.

3.4. Effect of polyatom substitution

Fig. 7 shows the correlation between NDR peak voltage of framework metal polyatom-substituted $H_nPW_{11}MO_{40}$ ($M = W^{6+}$, Mo^{6+}, V^{5+}) HPAs and Tanaka electronegativity of the mono-substituted polyatom, and between NDR voltage and reduction potential of $H_nPW_{11}MO_{40}$ ($M = W^{6+}$, Mo^{6+}, V^{5+}) samples. Reduction potentials of $H_nPW_{11}MO_{40}$ ($M = W^{6+}$, Mo^{6+}, V^{5+}) HPAs were taken from the literature [33,57]. The NDR peak voltages of $H_nPW_{11}MO_{40}$ ($M = W^{6+}$, Mo^{6+}, V^{5+}) arrays

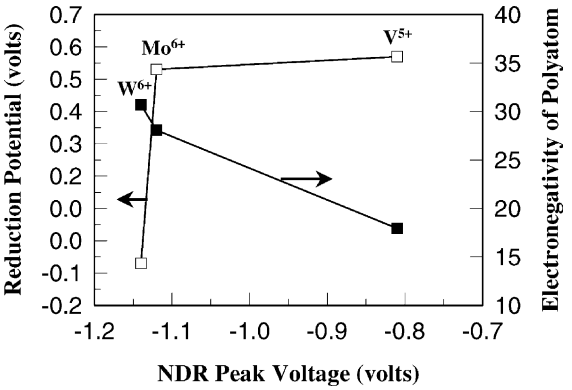

Fig. 7. Correlation between NDR peak voltage of polyatom-substituted $H_nPW_{11}MO_{40}$ ($M = W^{6+}$, Mo^{6+}, V^{5+}) HPAs and Tanaka electronegativity [55] of the mono-substituted polyatom (filled squares), and between NDR voltage and reduction potential [33,57] of $H_nPW_{11}MO_{40}$ ($M = W^{6+}$, Mo^{6+}, V^{5+}) samples (open squares).

appeared at less negative values with increasing reduction potential of the HPAs and decreasing electronegativity of the polyatom. Again this result is consistent with our finding that more reducible HPAs show NDR behavior at less negative applied voltages in their tunneling spectra. What is surprising about the results in Fig. 7 is that the trends of polyatom electronegativity with respect to NDR peak voltage and reduction potential of polyatom-substituted HPAs are the opposite of those seen for the cation-exchanged HPAs (Fig. 5) and heteroatom-substituted HPAs (Fig. 6).

In fact, the effect of polyatom substitution on the NDR peak voltage and reduction potential of HPAs is somewhat complicated. In our STM investigation on the vanadium-substituted $H_{3+x}PMo_{12-x}V_xO_{40}$ ($x = 0$–3) HPAs [43], it was observed that NDR peak voltages of these HPAs did not vary monotonically with the number of vanadium ions substituted (note that vanadium is less electronegative than molybdenum). Instead, the NDR peak appeared at the lowest negative voltage when $x = 2$. Nonetheless, NDR peak voltages were well correlated with reduction potentials across the composition range above. $H_5PMo_{10}V_2O_{40}$, which has the highest reduction potential, exhibited the lowest negative NDR voltage. Other framework substitutions produced monotonic variation of reduction potential and NDR peak position. In an STM investigation of polyatom-substituted $H_3PMo_{12-x}W_xO_{40}$ ($x = 0$, 3, 6, 9, 12) HPAs [43], it was observed that NDR peak voltages of these HPAs shifted to less negative values and their reduction potentials increased in a monotonic fashion with increasing Mo content. Once again, the correlation between NDR peak voltages and reduction potentials established for these polyatom-substituted HPAs was consistent. When considering that molybdenum is less electronegative than tungsten, the dependence of NDR peak voltage on the polyatom electronegativity observed for $H_3PMo_{12-x}W_xO_{40}$ ($x = 0$, 3, 6, 9, 12) HPAs shows the same trend as that observed for $H_nPW_{11}MO_{40}$ ($M = W^{6+}$, Mo^{6+}, V^{5+}) HPAs (Fig. 7). That is, NDR peaks of HPAs appeared at less negative applied voltages with decreasing Tanaka electronegativity of the substituted polyatom.

A molecular orbital study [61] for $H_nPM_{12-x}V_xO_{40}$ ($M = Mo^{6+}$, W^{6+}; $x = 0$–3) HPAs revealed that the energy gap between the highest occupied and the lowest unoccupied orbitals was consistent with reduction potential of the HPAs; the more reducible HPAs showed the smaller energy gaps. That study [61] also confirmed the results of the previous studies [59,60] that the HOMO for all HPAs consists primarily of nonbonding p-orbitals on the oxygens of the HPAs, while the LUMO consists of an antibonding combination of d-orbitals on the metal centers and p-orbitals on the neighboring bridging oxygens. Thus, substitution of V ions into either the Mo or W framework does not affect the energies of the HOMOs since they are almost entirely centered on the oxygens. The same substitution however does stabilize the LUMOs because these orbitals derive substantially from V d-orbitals which have been assumed to be more stable than those of Mo and W. This indicates that electrons added to the V-substituted HPAs should be localized on the vanadium centers, as evidenced from an ESR study [62]. Therefore, it can be inferred that electrons added to the polyatom-substituted $H_nPW_{11}MO_{40}$ ($M = W^{6+}$, Mo^{6+}, V^{5+}) HPAs are localized on the less electronegative metal center. The less electronegative polyatom in the $H_nPW_{11}MO_{40}$ ($M = W^{6+}$, Mo^{6+}, V^{5+}) HPAs is much more efficient in the role of electron localization.

One more interesting finding is that the dependencies of NDR peak voltage and reduction potential of $H_nPW_{11}MO_{40}$ ($M = W^{6+}$, Mo^{6+}, V^{5+}) HPAs on the electronegativity of the mono-substituted polyatom (Fig. 7) were exactly the same as those observed for ammonium salts of Wells–Dawson-type heteropoly oxofluorotungstates [63] with different mono-substituted polyatoms, $(NH_4)_nMW_{17}O_{56}F_6NaH_4$ ($M = Mn^{2+}$, Cu^{2+}, Mn^{3+}, Fe^{3+}) [64]. Tanaka electronegativity of the mono-substituted polyatom was in the order $Mn^{2+} < Cu^{2+} < Mn^{3+} < Fe^{3+}$, and the reduction potentials of the Wells–Dawson-type HPAs increased and NDR peak voltages appeared at less negative values with decrease in the electronegativity of the mono-substituted polyatom [64].

4. Conclusions

STM investigation of surface properties of nanostructured HPA monolayers was carried out to relate nanoscale properties to bulk redox properties of HPAs. Keggin-type HPAs with different counter-cation, polyatom and heteroatom substitutions were examined for

this purpose. All HPA samples studied in this work formed well-ordered monolayer arrays and exhibited negative difference resistance (NDR) behavior in their tunneling spectra. The observed NDR peak voltages were correlated with the reduction potential of HPAs and with the electronegativity of the mono-substituted metal atom. The NDR peak voltages observed for both cation-exchanged and heteroatom-substituted HPAs appeared at less negative values with increasing reduction potential of the HPAs and increase in the electronegativity of counter-cation and heteroatom. However, the dependencies of polyatom electronegativity on the NDR peak voltage and reduction potential of polyatom-substituted HPAs were the opposite of those observed for cation-exchanged and heteroatom-substituted HPAs; the NDR peak voltages of polyatom-substituted HPAs appeared at less negative values with increasing reduction potential of the HPAs and decreasing electronegativity of the polyatom. In spite of the different effect of polyatom substitution versus cation and heteroatom substitution, all these results consistently support the conclusion that the more reducible HPAs show NDR behavior at less negative applied voltages. It may therefore be feasible to utilize NDR peak voltages to predict surface redox properties, and thus as a correlating parameter with which to construct Balandin "volcano" plots for HPA-catalyzed selective oxidation reactions.

Acknowledgements

The authors thank Prof. C.L. Hill at Emory University for providing several of the HPA samples. The Topometrix TMX 2010 was acquired via an equipment grant from the US Department of Energy. In Kyu Song acknowledges fellowship support from the Seoam Scholarship Foundation.

References

[1] D.L. Carroll, R. Czerw, D. Tekeleab, D.W. Smith Jr., Langmuir 16 (2000) 3574.
[2] M. Böhringer, K. Morgenstern, W.-D. Schneider, M. Wühn, C. Wöll, R. Berndt, Surf. Sci. 444 (2000) 199.
[3] M. Edelwirth, J. Freud, S.J. Sowerby, W.M. Heckl, Surf. Sci. 417 (1998) 201.
[4] J. Noh, M. Hara, Langmuir 16 (2000) 2045.
[5] H. Tomimoto, R. Sumii, N. Shitota, S. Yagi, M. Taniguchi, T. Sekitani, K. Tanaka, J. Vac. Sci. Technol. B 18 (2000) 2335.
[6] F. Besenbacher, Rep. Prog. Phys. 59 (1996) 1737.
[7] F.M. Leibsle, P.W. Murray, N.G. Condon, G. Thornton, J. Appl. Phys. D 30 (1997) 741.
[8] S. Chiang, Chem. Rev. 97 (1997) 1083.
[9] P. Cernota, K. Rider, H.A. Yoon, M. Salmeron, G.A. Somorjai, Surf. Sci. 445 (2000) 249.
[10] H.J. Lee, W. Ho, Phys. Rev. B 61 (2000) R16347.
[11] A. Steltenpohl, N. Memmel, Surf. Sci. 443 (1999) 13.
[12] B.C. Stipe, M.A. Rezaei, W. Ho, S. Gao, M. Persson, B.I. Lundqvist, Phys. Rev. Lett. 78 (1997) 4410.
[13] Q. Chen, C.C. Perry, B.G. Frederick, P.W. Murray, S. Haq, N.V. Richardson, Surf. Sci. 446 (2000) 63.
[14] S.L. Silva, A.A. Patel, T.M. Pham, F.M. Leibsle, Surf. Sci. 441 (1999) 351.
[15] M. Valden, X. Lai, D.W. Goodman, Science 281 (1998) 1647.
[16] A. Bettac, L. Koller, V. Rank, K.H. Meiwes-Broer, Surf. Sci. 404 (1998) 475.
[17] M.K.-J. Johansson, S.M. Gray, L.S.O. Johansson, J. Vac. Sci. Technol. B 14 (1996) 1015.
[18] M.S. Kaba, I.K. Song, M.A. Barteau, J. Phys. Chem., in press.
[19] B.C. Stipe, M.A. Rezaei, W. Ho, Science 280 (1998) 1732.
[20] M.T. Pope, A. Müller (Eds.), Polyoxometalates: from Platonic Solids to Anti-retroviral Activity, Kluwer Academic Publishers, Dordrecht, The Netherlands, 1994.
[21] C.L. Hill (Guest Ed.), Chem. Rev. 98 (1) (1998).
[22] J.F. Keggin, Nature 131 (1933) 908.
[23] R. Neumann, Prog. Inorg. Chem. 47 (1998) 317.
[24] M. Misono, Catal. Rev.-Sci. Eng. 29 (1987) 269.
[25] I.V. Kozhevnikov, Catal. Rev.-Sci. Eng. 37 (1995) 311.
[26] C.L. Hill, C.M. Prosser-McCartha, Coord. Chem. Rev. 143 (1995) 407.
[27] Y. Onoue, Y. Miztani, S. Akiyama, Y. Izumi, Chemtech 8 (1990) 432.
[28] T. Yamada, Petrotech. 13 (1990) 627.
[29] S.S. Lim, Y.H. Kim, G.I. Park, W.Y. Lee, I.K. Song, H.K. Youn, Catal. Lett. 60 (1999) 199.
[30] A. Aoshima, S. Tonomura, S. Yamamatsu, Polym. Adv. Technol. 2 (1990) 127.
[31] H. Mori, N. Mizuno, M. Misono, J. Catal. 131 (1990) 133.
[32] A.W. Stobbe-Kreemers, R.B. Dielis, M. Makkee, J.J.F. Scholten, J. Catal. 154 (1995) 175.
[33] T. Okuhara, N. Mizuno, M. Misono, Adv. Catal. 41 (1996) 113.
[34] B. Dawson, Acta Cryst. 6 (1953) 113.
[35] R.G. Finke, M.W. Droege, Inorg. Chem. 32 (1983) 1006.
[36] M.H. Alizadeh, S.P. Harmalker, Y. Jeannin, J. Martin-Frere, M.T. Pope, J. Am. Chem. Soc. 107 (1985) 2662.
[37] M.S. Kaba, I.K. Song, D.C. Duncan, C.L. Hill, M.A. Barteau, Inorg. Chem. 37 (1998) 398.
[38] B.A. Watson, M.A. Barteau, L. Haggerty, A.M. Lenhoff, R.S. Weber, Langmuir 8 (1992) 1145.
[39] I.K. Song, M.S. Kaba, G. Coulston, K. Kourtakis, M.A. Barteau, Chem. Mater. 8 (1996) 2352.

[40] M.S. Kaba, I.K. Song, M.A. Barteau, J. Phys. Chem. 100 (1996) 19577.
[41] M.S. Kaba, I.K. Song, M.A. Barteau, J. Vac. Sci. Technol. A 15 (1997) 1299.
[42] M. Kinne, M.A. Barteau, Surf. Sci. 447 (2000) 105.
[43] I.K. Song, M.S. Kaba, M.A. Barteau, W.Y. Lee, Catal. Today 44 (1998) 285.
[44] I.K. Song, R.B. Shnitser, J.J. Cowan, C.L. Hill, M.A. Barteau, Inorg. Chem., in press.
[45] I.K. Song, M.S. Kaba, M.A. Barteau, J. Phys. Chem. 100 (1996) 17528.
[46] M.S. Kaba, M.A. Barteau, W.Y. Lee, I.K. Song, Appl. Catal. A 194 (2000) 129.
[47] D.A. Bonnel, Scanning Tunneling Microscopy and Spectroscopy, VCH, New York, 1993.
[48] H.-J. Müssig, D. Krüger, S. Hinrich, P.O. Hansson, Surf. Sci. 314 (1994) L884.
[49] A.G. Petukhov, D.O. Demchenko, A.N. Chantis, J. Vac. Sci. Technol. B 18 (2000) 2109.
[50] M. Ai, Appl. Catal. 4 (1982) 245.
[51] T. Okuhara, T. Nishimura, H. Watanabe, M. Misono, J. Mol. Catal. 74 (1994) 247.
[52] M.T. Pope, Heteropoly and Isopoly Oxometalates, Springer, New York, 1983.
[53] G.M. Brown, M.R. Noe-Spirlet, W.R. Busing, H.A. Levy, Acta Cryst. B 33 (1977) 1038.
[54] H. Hayashi, J.B. Moffat, J. Catal. 77 (1982) 473.
[55] K. Tanaka, A. Ozami, J. Catal. 8 (1967) 1.
[56] H.C. Kim, S.H. Moon, W.Y. Lee, Catal. Lett. (1991) 447.
[57] J.J. Alternau, M.T. Pope, R.A. Prados, H. So, Inorg. Chem. 14 (1975) 417.
[58] M. Sadakane, E. Steckhan, Chem. Rev. 98 (1998) 219.
[59] K. Eguchi, T. Seiyama, N. Yamazoe, S. Katsuki, H. Taketa, J. Catal. 111 (1988) 336.
[60] H. Taketa, S. Katsuki, K. Eguchi, T. Seiyama, N. Yamazoe, J. Phys. Chem. 90 (1986) 2959.
[61] R.S. Weber, J. Phys. Chem. 98 (1994) 2999.
[62] M.M. Mossoba, C.J. O'Connor, M.T. Pope, E. Sinn, G. Hervé, A. Tézé, J. Am. Chem. Soc. 102 (1980) 6864.
[63] S.H. Wasfi, C.E. Costello, A.L. Rheingold, B.S. Haggerty, Inorg. Chem. 30 (1991) 1788.
[64] M.S. Kaba, I.K. Song, S.H. Wasfi, M.A. Barteau, J. Electrochem. Soc., in press.